William H. Jolly
William P. Schonberg
Civil & Environmental Engineering Department
The University of Alabama in Huntsville
Huntsville, AL 35899, USA

Analytical Prediction of Hole Diameter in Thin Plates Due to Hypervelocity Impact of Spherical Projectiles

A first-principles-based model is presented for calculating the hole diameter resulting from the normal hypervelocity impact of a spherical aluminum projectile on a thin aluminum plate. One-dimensional shock theory is used to predict the creation and attenuation of Hugoniot pressures along the plate surface. Pressures are translated into the plate thickness by calculating intersecting positions of advancing shock fronts and centered-fan rarefaction waves. The radial position at which the shock pressure equals a predetermined value is defined to be the hole diameter. The model was calibrated by determining this critical value for aluminum-on-aluminum impacts using several hundred data points. A residuals analysis indicated some inherent problems with the model. Two empirical factors were added to account for thin plate and two-dimensional shock dissipation effects. The predictions of the adjusted model are shown to compare well with predictions of several empirical hole diameter models.

INTRODUCTION

The study of hypervelocity impacts against aluminum structures has its genesis in the early days of the space program. Spacecraft exterior structures continue to be designed to protect astronauts and critical components from the hazards of the near-earth space environment. This environment is fluent with both naturally occurring and man-made particles. At present, man-made particles present the larger threat to operations in low earth orbit due to their relatively high density (on the order of 2.7 gm/cm^3, or approximately that of aluminum) and their speed (10–12 km/s, on average). The most utilized spacecraft protective wall design was initially suggested by Fred Whipple (1947). The design consists of a dual wall system where an incoming particle would impact a thin exterior wall (also referred to as a "bumper") and would be sufficiently shocked to cause fragmentation, liquefaction, and perhaps vaporization of both the projectile and the bumper materials (see, e.g., Madden, 1967; Nysmith, 1968; Maiden, McMillan and Sennett, 1965).

During the spacecraft design process, an optimum bumper thickness must be determined to minimize the launch weight and maximize protection. This optimum thickness can be determined through several techniques depending upon the specific aspect of the design being considered. However, no matter which parameter is used to constrain the optimization, a fast-running hole diameter prediction tool is required to characterize the impact event. If the design is to be conservative, such a tool can be used to determine the

Received 26 March 1996; Revised 9 September 1997.
Shock and Vibration, Vol. 4, No. 5,6, pp. 379–390 (1997)
ISSN 1070-9622/97/$8.00

amount of material added to the debris cloud created as a result of the perforation of the bumper. This information is then used to determine the magnitude of the debris cloud loading on the inner spacecraft wall.

Traditional approaches to determine the hole diameter in a thin plate due to a high speed impact typically fall into two broad categories: empirical and numerical. Empirical approaches involve the use of an equation that was obtained through a curve fitting exercise using test data. Such equations have two severe limitations: 1) they provide no information with regard to the phenomena involved; and 2) they are limited in their use to impact conditions, materials, etc., that fall within the realm of the parameters used to obtain the equations. Alternatively, numerical analyses through the use of hydrocodes provide a detailed description of the physical processes involved and are applicable to a much wider class of problems. Hydrocodes are finite difference or finite element codes that are used to study shock wave propagation in solids. However, the time element involved in hydrocode analyses normally precludes their use when it is required to obtain hole diameters for a large number of impact conditions, material combinations, or plate thicknesses. Thus, an analytical model of hole formation due to a high speed impact is required that is both fast-running and based on physical principles.

While a number of analytical models currently exist for radial hole growth in thick and thin plates, these models typically consider cylindrical projectiles with relatively large length-to-diameter ratios (see Walters and Scott, 1985; and Walters and Zukas, 1989, for exhaustive literature citations). By considering a cylindrical geometry and the symmetries associated therein, the complications associated with the impact of compact or spherical projectiles are avoided. Analytical models that do consider spherical projectiles are restricted to low velocity (i.e., non-penetrating) impacts. Thus, there exists a need to develop an analytical hole diameter model for the high speed impact of a spherical projectile on a thin plate.

In an attempt to address this need, this paper presents the development of an first-principles-based hole diameter model for the high speed impact of a spherical aluminum projectile on a thin aluminum target plate. As such, the model would be directly applicable to the modeling of orbital debris impacts on thin spacecraft walls or bumpers. The analysis makes use of one-dimensional shock wave propagation and attenuation phenomenology (see, e.g., Fowles, 1960; Chou, 1965). The basic concept in this analysis is to consider the Hugoniot pressure generated by a high speed impact and to predict the radial decay of that pressure as the shock wave travels away from the point of impact. At some radial distance from the point of impact, the pressure in the plate will drop below a certain critical value. The position at which this occurs would correspond to the hole diameter. The hole diameter prediction model is validated by comparing its predictions against those obtained in previous experimental studies. A parametric analysis is also performed to determine the overall characteristics displayed by the model. While the model is developed and validated for aluminum-on-aluminum impacts, the methodology presented can readily be adapted to other material combinations.

SHOCK LOADING AND RELEASE ANALYSIS

Consider a spherical projectile with diameter 'd' (radius 'R') normally impacting a flat plate with thickness 'h'. A spherical projectile is considered in this analysis because the vast majority of experimental studies, the results of which are used to calibrate the model, used spherical projectiles. As the velocities of interest are on the order of several km/s, the model to be developed will consist of shock dominated processes. Upon impact, shock waves are set up in the projectile and target materials. As the shock waves propagate, the projectile and target materials are heated adiabatically and non-isentropically. The release of the shock pressures occurs isentropically through the action of rarefaction waves that are generated as the shock waves interact with the free surfaces of the projectile and target. This process can cause the projectile and target materials to fragment, melt or vaporize, depending on the material properties, geometry, and the impact velocity.

At very early times during the impact event, only the area in the immediate vicinity of the impact site is affected by the impact. For the projectile and target geometries considered in this study, the shock waves can be considered to be initially planar. This simplification allows one-dimensional relationships to be used for analyzing the creation and release of shock pressures. The shock pressures, energies, etc., in the projectile and target materials are calculated using the three 1-D shock-jump conditions, a linear relationship between the shock wave velocity and particle velocity in each material, and continuity of pressure and velocity at the projectile/target interface. Solving the resulting equations simultaneously yields expressions for projectile and target particle velocities which are then used to calculate shock velocities, pressures, internal energies, and material densities after the passage of a shock wave.

While the shock loading of a material is an irreversible process that results in an increase of the internal energy of the shocked material, the release of a shocked material occurs isentropically along an 'isentrope' or 'release adiabat'. The difference between the area under the isentrope and the energy of the shocked state is the amount of residual energy that remains in the material and can cause the material to melt or even vaporize. In order to calculate the release of the projectile and target materials from their respective shocked states, an appropriate equation-of-state is needed for each material. To keep the analysis relatively simple, the Mie-Gruneisen equation-of-state was used in this study (Walsh et al., 1957; Rice et al., 1958). The following section presents a summary of the method to be used for the one-dimensional attenuation of the shock pressures generated by the initial impact. It is then shown how this procedure can be applied to the attenuation of the impact pressures in a thin plate along the surface of the plate.

SURFACE ATTENUATION OF SHOCK PRESSURES

One-Dimensional Attenuation Scheme

When a spherical projectile normally impacts a plate, a shock is produced in the target plate that travels away from the point of impact. Attenuation of the shock wave begins when that shock intersects a free surface. The adjacent target surface surrounding the projectile is assumed to be the free boundary where attenuation of the shock at the surface of the target begins. The one-dimensional shock and rarefaction fan interaction illustrated in Fig. 1 is used to model shock wave attenuation following spherical projectile impact, where point O indicates the position of the initial impact, point A is the position where shock wave attenuation begins, and point I is the origination point of a centered rarefaction such that the intersection of the head of the rarefaction and the shock occurs at point A. As did Chou (1965), we assume that the head of the rarefaction wave travels at a constant speed given by the sum of the particle velocity and the local speed of sound, and that this sum is constant along each characteristic line. Point I is determined from the positions of points A and O and the slopes of the lines which are defined by the reciprocals of the initial shock velocity U_s and the initial rarefaction wave velocity $z = u_p + c$, where u_p is the initial particle velocity and c is the material bulk speed of sound. Following the procedure in Fowles (1960) and Chou (1965), the equations used to characterize the attenuation process depicted in Fig. 1 are obtained as follows. To begin, we write the equation of a characteristic line as

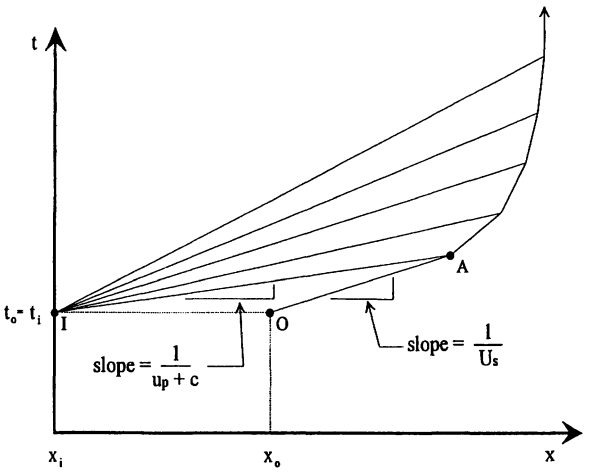

FIGURE 1 The x–t diagram for a centered rarefaction fan overtaking a shock wave.

$$x - x_i = (u_p + c)(t - t_i) = z(t - t_i) \qquad (1)$$

where t_i is the time at which the centered rarefaction emanates from its origination point. After differentiating each side of this equation with respect to z, we have

$$\frac{dx}{dz} = (t - t_i) + z\frac{dt}{dz}. \qquad (2)$$

Noting that $\frac{dx}{dt} = U_s$ and applying the chain rule to the left hand side of Eq. (2) yields

$$U_s\frac{dt}{dz} = (t - t_i) + z\frac{dt}{dz}. \qquad (3)$$

Grouping the terms and separating the variables results in the following integral:

$$\int_{z_1}^{z} \frac{dz}{U_s - z} = \int_{t_a}^{t} \frac{dt}{t - t_i} \qquad (4)$$

where t_a is the time at which the rarefaction wave first intersects the shock wave and z_1 is the initial rarefaction wave speed. As did Chou (1965), we must assume a quadratic relationship between U_s and z of the following form:

$$U_s = a_1 + a_2 z + a_3 z^2. \qquad (5)$$

Substituting Eq. (5) into Eq. (4) and evaluating the integrals yields the following expression for t as a function of z:

$$t = t_i + (t_a - t_i)\left[\left(\frac{X + z}{X + z_1}\right)\left(\frac{Y + z_1}{Y + z}\right)\right]^{D/a_3}, \qquad (6)$$

where

$$X = \frac{1}{2}\left[\sqrt{\left(\frac{a_2 - 1}{a_3}\right)^2 - \frac{4a_1}{a_3}} + \frac{(a_2 - 1)}{a_3}\right], \quad (7)$$

$$Y = -\frac{1}{2}\left[\sqrt{\left(\frac{a_2 - 1}{a_3}\right)^2 - \frac{4a_1}{a_3}} - \frac{(a_2 - 1)}{a_3}\right], \quad (8)$$

$$D = \frac{1}{Y - X}. \quad (9)$$

The coefficients a_1, a_2, and a_3 are obtained by performing a linear least squares curve fit between shock speed U_s and characteristic speed $z = c + u_p$. Corresponding values of U_s and z are obtained from assumed values of u_p by using the linear $U_s - u_p$ relationship from the shock loading analysis and the definition of the characteristic velocity z. For aluminum-on-aluminum impacts, it is found that $a_1 = 1.484$, $a_2 = 0.652$, and $a_3 = 9.381 \times 10^{-4}$. We now proceed to determine the locations of points A, I, and O on the surface of the target plate and show how the equations developed in this section are applied to the problem of thin plate impact.

Application to Thin Plate Impact

Consider the kinematics of a sphere impacting a thin target plate as shown in Fig. 2. Point O with coordinates (x_o, t_o) is simply defined as the position of the impact on the target plate and the time at which it occurs, respectively. The location on the target surface at which attenuation of the shock propagation begins, i.e., point A which is located at a distance ℓ from point O, is obtained by considering the formation of shock waves in the target plate as the projectile impacts the target plate upper surface.

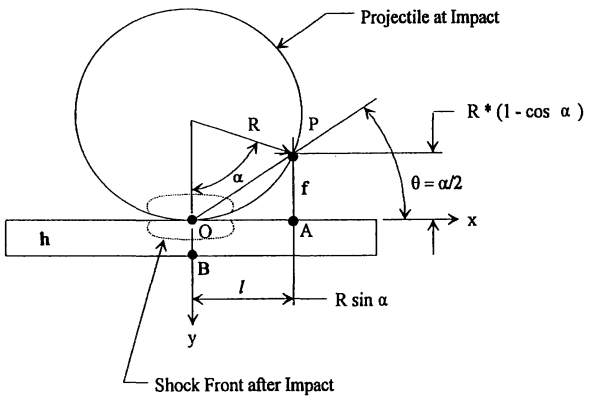

FIGURE 2 Geometry at the time of impact.

At early times, shocks are formed in the target plate prior to the arrival of the shock wave initiated at the point of impact. This nucleation of shock waves in a radial direction along the target surface slows down due to the spherical shape of the projectile. As time progresses, a point is reached where the initial shock created at point O eventually catches up with the creation of new shocks. This position corresponds to point A in Fig. 2, and it is at this point that the attenuation process begins. The target material contained within the cylinder of radius ℓ about the projectile centerline is continuously shocked by the incoming projectile material and therefore is considered to be completely removed from the target plate (i.e., the hole diameter is at least 2ℓ).

To determine the distance ℓ from point O to point A in Fig. 2, we assume that it defines the point along the upper surface of the target plate where the shock meets the incoming projectile material from point P. In this manner, the time required for the shock to traverse from the origin to point A in Fig. 2, t_{OA}, is the same as the time required for the corresponding point on the projectile, P, to move to the target surface or t_{PA}. These quantities may be written as

$$t_{OA} = \frac{R \sin\alpha}{U_s} = \frac{\ell}{U_s}, \quad (10)$$

$$t_{PA} = \frac{R(1 - \cos\alpha)}{V_0} = \frac{f}{V_0}. \quad (11)$$

Equating the two times yields the following expression for the angle α at which the shock begins to outrun the incoming projectile:

$$\alpha = 2\tan^{-1}\left(\frac{V_0}{U_s}\right). \quad (12)$$

Once α is known, the distance ℓ is calculated directly from

$$\ell = R \sin\alpha. \quad (13)$$

Thus, the coordinates of point A are given by $x_a = \ell$ and $t_a = \ell / U_s$.

Now that the position at which attenuation begins is known, the attenuation of the shock in the target plate is determined using Eqs. (1) and (6)–(10). This attenuation is assumed to occur along the upper surface of the target in a radial direction (i.e., the x direction in Fig. 2). However, in order to utilize Eqs. (1) and (6)–(10), the position of point I must still be determined. In the case of thin plate impact, shock wave rarefaction begins at a time almost immediately following the time of impact. Thus, since this model is being developed for thin plate impact, it is assumed that rarefaction does in fact begin at the time of initial impact,

that is, $t_i = t_o$. Then, by applying Eq. (1) to line $\overline{IA}$ in Fig. 1, the position of the rarefaction center can be written as

$$x_i = x_a - (t_a - t_i)z_1. \quad (14)$$

This completes the definition of point I as well.

Now that the locations of points A, I and O are known, the attenuation of the shock wave along the plate surface proceeds as follows. First, the initial rarefaction wave speed z_1 is decreased by a small amount Δz to a new amount z. The time at which this occurs is found using Eq. (6); the position along the plate surface at which this speed occurs is found using Eq. (1). Then, for the value of z being considered, the corresponding pressure can also be found provided that the relationship between p and z is known. This calculated pressure value is then compared against a critical pressure value. If the calculated pressure is less than the critical value, hole enlargement stops; if it exceeds the critical value, z is again decreased and the process is repeated.

For aluminum-on-aluminum impacts, the relationship between p and z is given by

$$p = 7.27\times10^{-4} - 5.57\times10^{-2}z + 9.96\times10^{-3}z^2 \quad (15)$$

where z is in km/s and p is in MBar. The coefficients in Eq. (15) are obtained in a manner similar to that used to obtain those in Eq. (5). For a given value of u_p, the corresponding value of p is determined from one-dimensional shock jump conditions while that of z is determined from its definition. A least squares fit between corresponding values of p and z then yields the coefficients given above in Eq. (15). We note that according to Eq. (15), $p = 0$ when $z = 5.58$ km/s. This value is only 4.3% larger than the value z should have when $p = 0$, that is, the bulk speed of sound in aluminum or 5.35 km/s. Hence, the curve-fit given by Eq. (15) is expected to agree reasonably well with the Hugoniot for aluminum, and has only a slight disagreement near $p = 0$.

The critical pressure value at which hole enlargement is presumed to cease is, in effect, a material property like yield stress or ultimate stress. In order for the model being developed to function in a predictive mode, this value must be a known quantity; like all other material properties, it must be determined experimentally. In this study this particular quantity is obtained by calibrating the analytical model. That is, model predictions of hole diameter are compared with experimental hole diameter measurements to determine the critical pressure value for the projectile/target plate material combination under consideration. The model is then run in its *predictive* mode to ascertain its accuracy in predicting hole diameter under a variety of different impact conditions which are not necessarily the same as those used in its calibration.

We note that up until now the thickness of the target has been ignored. We have developed, in effect, a model for predicting crater mouth diameter in a semi-infinite target. In order to account for thickness of a target, the model must be able to calculate attenuated shock pressures within the target. The following section presents the technique used to resolve the surface attenuation of the initial shock wave to locations within the thickness of the target plate.

CHARACTERISTIC SOLUTION INTO THE PLATE THICKNESS

Target Section Under Full Hugoniot Pressure

From the position where attenuation is defined to begin (point A in Fig. 3), a locus of points along a line as shown in Fig. 3 must exist, where the head of the rarefaction wave emanating from point A intersects the shock at positions within the target thickness. Curve 1 defines a region behind which all the target material is shocked to the initial Hugoniot pressure. Additional curves, such as Curve 2 shown in Fig. 3, that outline target regions affected by reduced attenuated pressures, can be defined in a similar manner. These curves can be readily defined if the shock front and the fan of rarefaction waves are assumed to be spherical. In determining the position of these two curves, two different approaches were used, one for each curve. Both approaches required the use of an iterative technique to solve relationships that cannot be solved directly. Curve 1 was constructed using time as the free parameter in the following manner.

Consider the arrangement shown in Fig. 4. As in Fig. 3, Curve 1 defines the portion of the target where

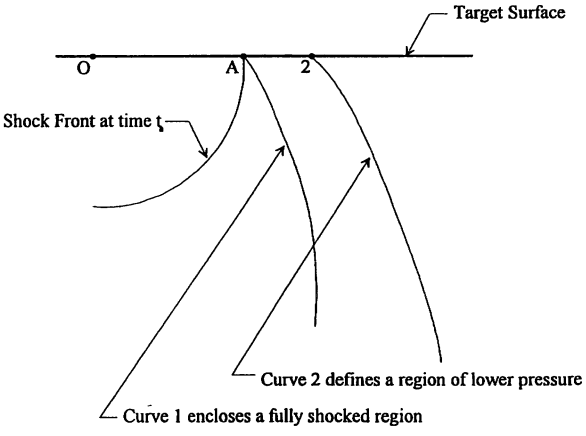

FIGURE 3 Regions of peak pressure.

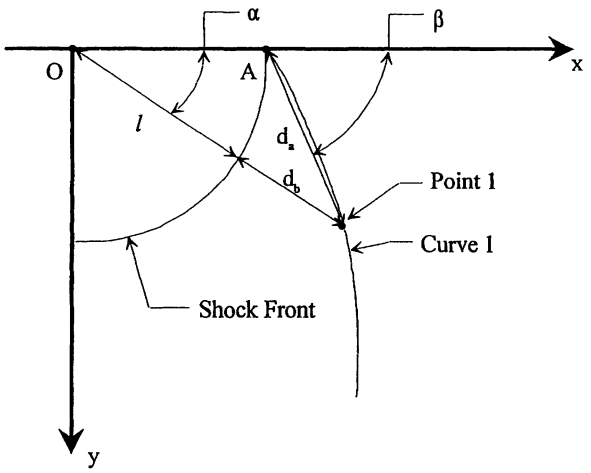

FIGURE 4 Schematic of locus of rarefaction – shock intersections.

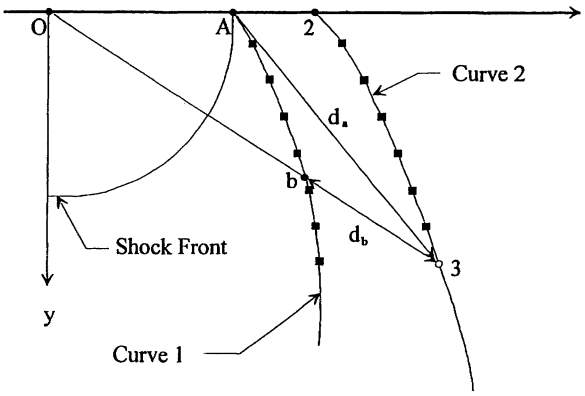

FIGURE 5 Schematic of Curve 2.

the full Hugoniot pressure occurs before it is attenuated. The coordinates of point 1 can be written as

$$y = d_a \sin\beta = (\ell + d_b)\sin\alpha, \tag{16}$$

$$x = \ell + d_a \cos\beta = (\ell + d_b)\cos\alpha. \tag{17}$$

Squaring and adding these equations results in

$$x^2 + y^2 = d_a^2 + \ell^2 + 2\ell d_a \cos\beta = (\ell + d_b)^2. \tag{18}$$

Solving the right hand side of Eq. (18) for β yields:

$$\cos\beta = \frac{2\ell d_b + d_b^2 - d_a^2}{2d_a\ell} \tag{19}$$

where d_a and d_b are defined as

$$d_a = (u_p + c)(t - t_a), \tag{20}$$

$$d_b = U_s(t - t_a). \tag{21}$$

Thus, once the quantity $t - t_a$ is known, then Eq. (19) defines the position of point 1 on Curve 1 with respect to point A. The entire locus of points that constitutes Curve 1 is thus found by using Eqs. (19)–(21) for small sequential increments of t above t_a.

Attenuated Pressure Curves

To determine Curve 2, it is noted that the area between Curves 1 and 2 illustrated in Fig. 3 defines a portion of the target where the pressure value never reaches the peak impact pressure. To determine the attenuation within the target, point 2 on the target surface and the positions of the locus of points where the second rarefaction wave intersects the reduced shock wave must be found. The general derivation of points that make up Curve 2 requires knowledge of the shock trajectory prior to arriving at a specific point. Once again, an iterative technique is required to determine the location of each point. Each curve is generated through a structured progression of point determinations that are dependent upon the location of the previous curves.

To set up the method of solution for curves subsequent to Curve 1, it is convenient to make the following designations corresponding to Fig. 5. Determining the location of point 3 is the focus of this derivation. The shock emanating from the origin has been reduced in pressure by previous rarefaction interactions and, is intersected by a subsequent rarefaction at point 3. The precise location of the last shock interaction is indicated by the filled circle at point b. In this case the prior interaction was the first; however, this need not be the case in general. The positions of all prior solutions on the adjacent curve (Curve 1 in this example) are indicated by filled squares.

In Fig. 5, the pressure history for the shock trajectory is known because all the points that comprise the adjacent curve have already been determined. In addition, the times corresponding to each of those points are known. The y coordinates of all corresponding points are pre-set to be the same for each curve. This constant grid spacing in the y direction is set during the determination of the first curve and is a function of the target thickness. Thus, as a result of setting up this grid spacing, the y coordinate of point 3 is known.

The reduced shock arrives at point 3 at the same instant in time that the second rarefaction wave arrives from point A. The approach taken was to assume a value for the x coordinate (beginning with the x coordinate of the previous point on Curve 2), to solve for the times required for the intersecting waves to transit

from to point 3, and to check for equality in that transit time. In order to determine the time for the shock transit, the position and time corresponding to point b is determined using a linear interpolation between the two known points on the previous curve. With this position and time known, a simple minimization of the delta time with respect to the x position of the desired point provides a solution. It is noted that due to the approximations invoked for determining the location of point b and the stepwise reduction in pressure, small increments in y and z are necessary to provide adequate solutions when using these techniques.

MODEL ADJUSTMENTS

Since there are a fair number of assumptions made in the preceding analysis, some adjustments to the model will be required to account for any discrepancies between analyses and experiments. The required adjustments will be incorporated during the calibration phase of the model development, which is discussed in the next section. The discussion here will concentrate on the anticipated short-comings of this model. An understanding of the source of these shortcomings will suggest where best to focus empirical modifications and will also indicate the areas where the model could be improved.

Velocity Effects

One of the assumptions made in the development of this model is that the expanding shock wave travels at constant speed. Since the shock propagation speed is a function of pressure, and since pressure is a function of radial expansion, the basic model will provide solutions that exhibit velocity dependencies. For calibration analyses where the predicted critical pressure at the edge of the actual hole is determined, the critical pressure will increase with impact velocity. In fact, since this is a one-dimensional shock calculation, higher impact velocities automatically result in higher shock velocities and, therefore, will also result in higher predicted peak pressures. In light of this reasoning, the hole diameters predicted by the model will increase rapidly as impact velocity increases. However, hole diameter should not increase rapidly with increasing impact velocity because of rarefaction from the back surface. In addition, if a thin plate perforated at an extremely high velocity is postulated, a particle in the target plate at the radius of the projectile would be, by definition, disrupted before any shock in the target could propagate beyond that radius.

In order to account for these effects, a method of altering the particle speed should be developed such that a continuous reduction in the associated Hugoniot pressure at the point in the target from which attenuation begins can be achieved as the impact velocity increases. A reduction in the particle velocity results in a corresponding reduction in the shock speed, the Hugoniot pressure and the compressed sound speed. The manipulation of the particle speed used herein is defined by

$$u_p|_a = u_p|_0 \left(\frac{\vec{V}_0 \cdot \vec{n}}{V_0} \right) \tag{22}$$

where $\vec{n}$ is the normal component of the projectile surface at the position where the onset of attenuation occurs. This will provide the actual Hugoniot pressure for low speed impacts and somewhat lower values for very high speed impacts when the projectile surface normal is perpendicular to the velocity vector (i.e., parallel to the plate).

Rear Surface Effects

In its basic form, the model developed herein ignores the rear surface of the target plate and assumes that the centered rarefaction fan emanating from the surface of the target is the only process affecting the shock. When the thickness of the target is less than the distance between the impact point and the origin of rarefaction fan (points O and A in Fig. 2, respectively), then the shock is also affected by rarefaction from the back side of the target. Referring to Fig. 2, in such a case, the shock would impact the rear surface of the target plate at point B before it reaches point A. The proper method of handling this situation would be to place the origin of the centered rarefaction at point B and attenuate the pressure from that point. This would not be possible within the framework of the current model because then the solution for the attenuation could not be obtained analytically. Therefore, to account for very thin targets, a position between the point of impact and point A would need to be determined to allow "early" attenuation in thin plate targets (i.e., those targets in which $\overline{OB} < \overline{OA}$).

One method of accomplishing this result is to set the position of A equal to the target thickness when the thickness is less than the distance to point A. Another method is to average the distances $\overline{OB}$ and $\overline{OA}$ to determine the point from which attenuation begins. The average value would provide a more continuous transition at thicknesses equal to the calculated position of A and would limit the rate at which the hole diameter decreases with respect to the target thickness. Hence, it is the average value method that is chosen for continued use in the development and implementation of the hole diameter prediction model.

RESULTS AND DISCUSSION

The model developed herein is verified by comparing its predictions to those of other empirically-based hole diameter prediction models. To determine the range of applicability for this model, a series of parametric evaluations were performed. The source of the experimental data used in this study is the NASA/Marshall Space Flight Center HITS Database (Schonberg et al., 1991). The range of the impact velocity for the aluminum-on-aluminum tests within this database is 2.0 to 7.6 km/s; the range of the h/d ratios is from 0.085 to 0.503.

Model Checkout and Adjustments

As indicated in the previous section, some adjustments to the basic model are anticipated to account for some of the simplifying assumptions. Before those modifications were made, the program was run in its basic form. The results of that preliminary analysis are provided in the next section, followed by a section describing the actual adjustments that were made to the model.

Preliminary Analysis An analysis was made using the basic model without any adjustments for a variety of plate thicknesses, projectile diameters and impact velocities. Each combination of thickness, diameter and velocity considered corresponded to an actual test for which a hole diameter data point was available. Shock pressures created by the initial impacts were attenuated with distance away from the impact points. For each combination of plate thickness, projectile diameter, and impact velocity (i.e., for each trial run), when the distance at which an attenuated pressure was calculated equaled the empirical hole radius value, the pressure at the center of the target thickness was noted and recorded. In this manner, a critical pressure value was obtained for each test. Figures 6–8 show the variation of these critical pressures as a function of plate thickness, projectile diameter, and impact velocity, respectively. An absolutely correct model would have displayed a constant value for the critical pressure in each of these figures. Figures 6 and 7 indicate a fairly large scatter in calculated critical pressure; however, no clear dependencies exist with respect to target thickness or projectile diameter.

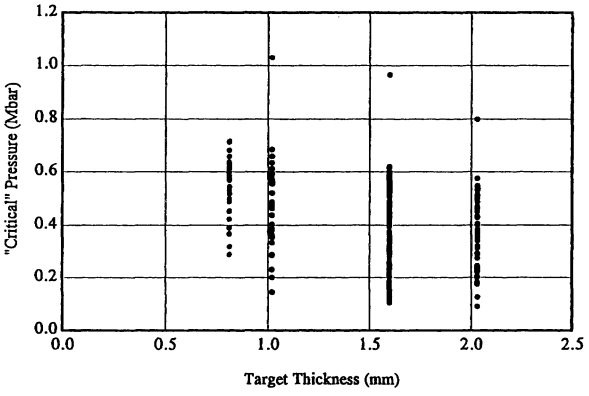

FIGURE 6 Basic model: Critical pressure versus target thickness.

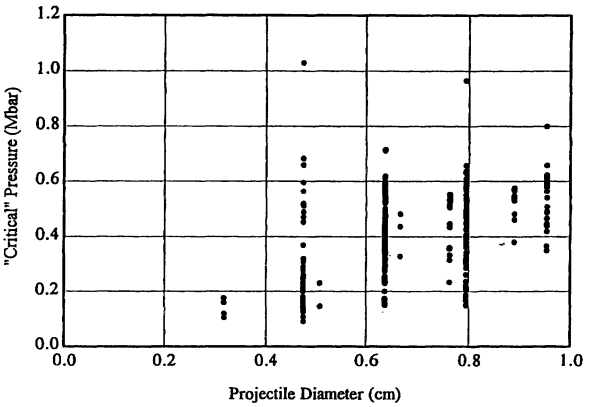

FIGURE 7 Basic model: Critical pressure versus projectile diameter.

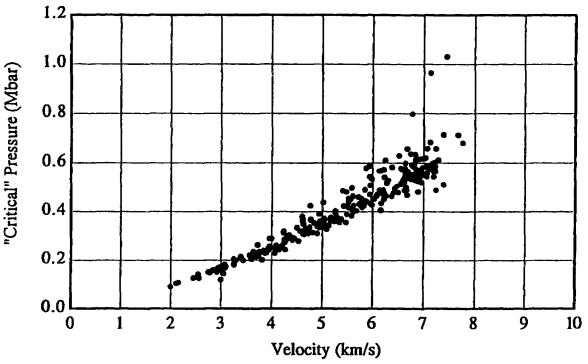

FIGURE 8 Basic model: Critical pressure versus velocity.

Figure 8, however, indicates a significant dependency with respect to velocity. This dependency can be overcome by fitting a curve through the data and using that estimation of pressure as a velocity dependent critical pressure value adjustment in the hole diameter prediction model. However, this method of resolving the dependency is not desirable for a number of reasons. First, the threshold pressure is probably more of a function of the impact pressure developed in the target than just the impact velocity. Second, it is hoped that the methodology developed herein can be made suitable for other material combinations. This added

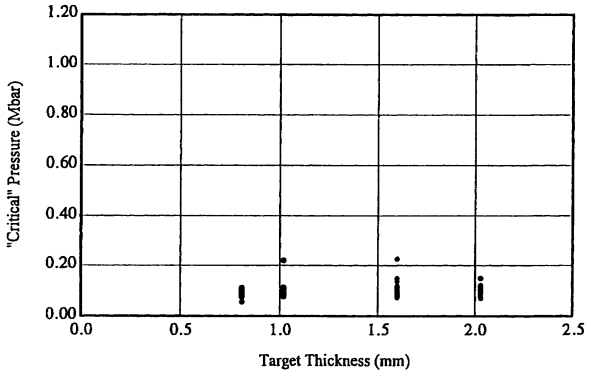

FIGURE 9 Final model: Critical pressure versus target thickness.

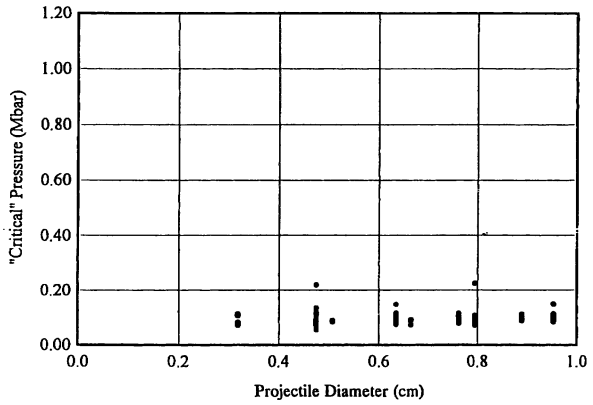

FIGURE 10 Final model: Critical pressure versus projectile diameter.

complexity in the modeling would make determination of a generalized threshold pressure function virtually impossible to obtain. Finally, this approach to removing the velocity dependence would merely consist of developing an empirical model to account for the current inadequacies, which would transform the overall model itself into yet another empirical hole diameter model. The preferred approach is, therefore, to correct the physical model itself.

Model Adjustments Adjustments to account for velocity and near surface effects were incorporated into the hole diameter model and the analysis was repeated; Figures 9–11 present the results. The plots in Figures 9–11 use the same scale as the previous figures to indicate the relative improvement with respect to each independent variable. Figures 9,10 indicate a marked reduction in the observed scatter as predicted by the adjusted model. In these figures the dependency of critical pressure on target thickness and projectile diameter is seen to be significantly reduced. In addition, Figure 11 indicates virtually no velocity dependence in the

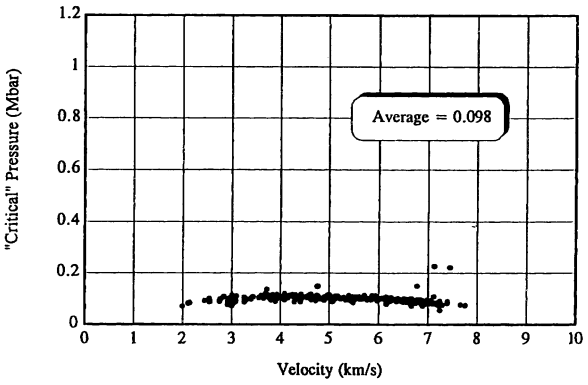

FIGURE 11 Final model: Critical pressure versus velocity.

critical pressure. Therefore, the analysis appears to indicate that the adjustments made to the model have resulted in an improved prediction tool. The 0.098 MBar average critical pressure value in Figure 11 is approximately 50 times the ultimate strength of aluminum 6061-T6. While some discrepancy was anticipated from the use of the one-dimensional schemes, such a large difference was not. The model must be calibrated to include adjustment of the critical pressure value for specific projectile/target material combinations.

Prediction and Correlation

Hole diameters were predicted for 277 aluminum-on-aluminum impact tests contained in the HITS Database and compared against the test values. The relative errors of model predictions were found to be within ±20% of the experimental measurements for ~99% of the data; a residual analysis indicated the multiple correlation coefficient to be 0.70 for the model developed herein. While a 20% relative error may be considered to be fairly large, this scatter is not unusual and is in fact comparable with that obtained from other models that are considered to be accurate to within the natural scatter in the data (Gehring, 1970). Hence, it may be surmised that the scatter obtained using the model developed herein is likely the result of random errors associated with the perforation event as well as with the experimental measurements.

Comparison to Other Models

In a literature search for other hole diameter models, four empirical predictor equations were found that were applicable to hypervelocity impact against thin plates (Nysmith, 1968; Gehring, 1970; Swale, 1970;

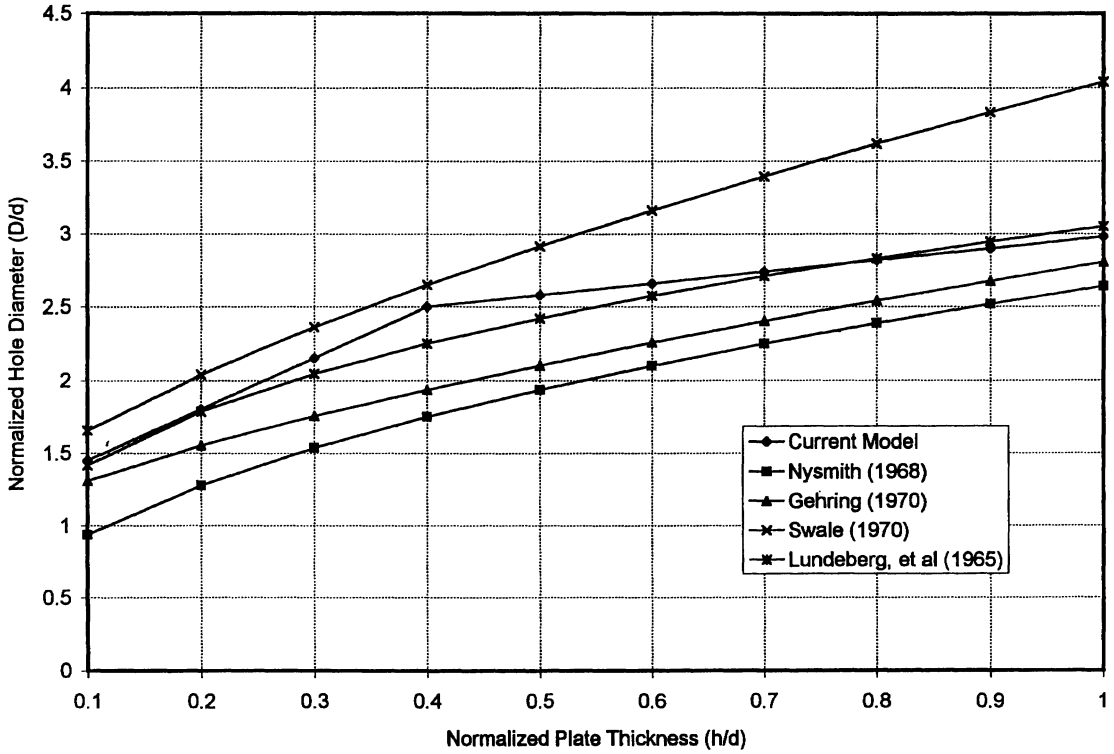

FIGURE 12 Normalized hole diameter vs. normalized plate thickness: Comparison of model predictions to Nysmith (1968), Gehring (1970), Swale (1970), and Lundeberg et al. (1965) for a 4.0 km/s impact velocity.

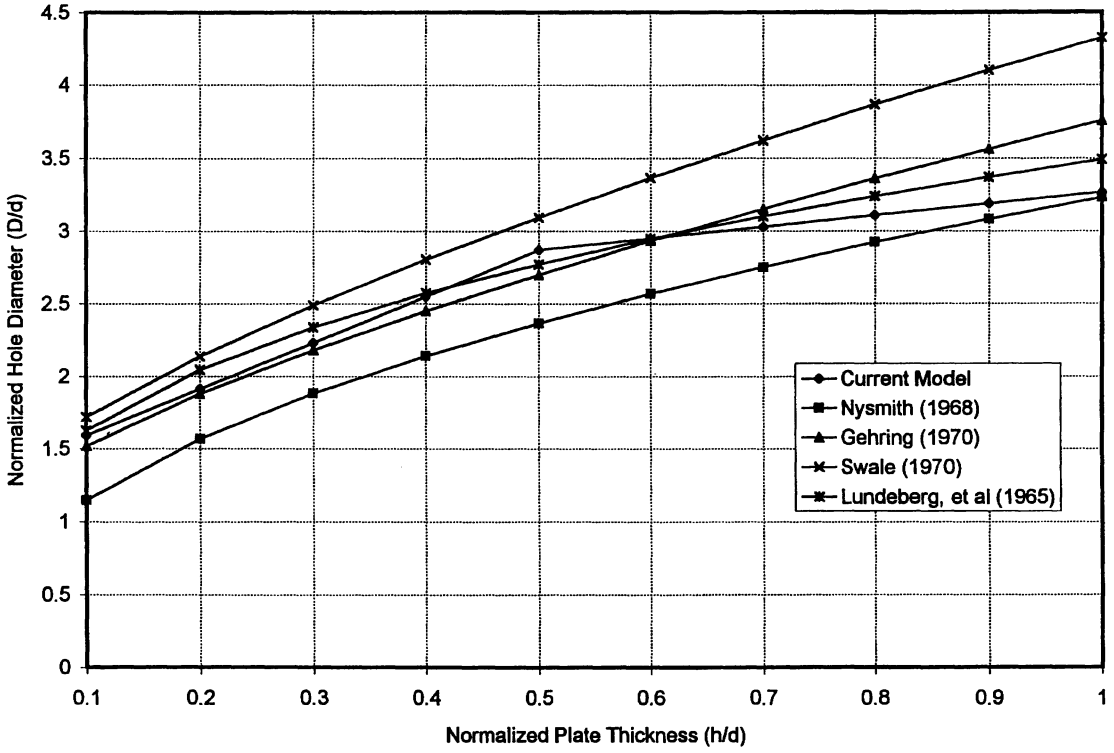

FIGURE 13 Normalized hole diameter vs. normalized plate thickness: Comparison of model predictions to Nysmith (1968), Gehring (1970), Swale (1970), and Lundeberg et al. (1965) for a 6.0 km/s impact velocity.

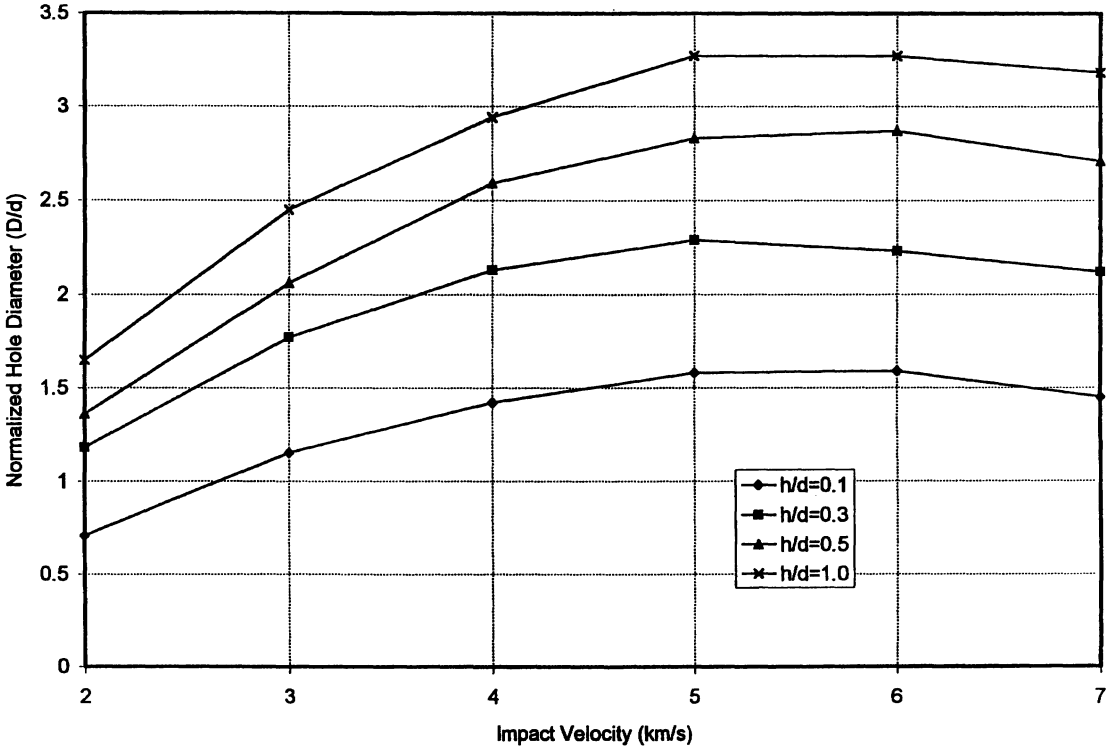

FIGURE 14 Normalized hole diameter versus impact velocity.

Lundeberg, Stern and Bristow, 1965). Numerical results were obtained for various impact velocities and h/d ratios. Figures 12 and 13 show comparisons of the results obtained using the model developed herein and these other models for impact velocities of 4 and 6 km/s, respectively. Based on the results obtained herein, the current model appears to be in good agreement with a large set of experimental data as well as several other empirical models generated from numerous experimental studies.

Parametric Evaluation

A parametric study using the hole diameter prediction model developed herein was performed by systematically varying target thickness and impact velocity for a fixed projectile diameter. The results were then plotted to reveal the parametric nature of the model. Figure 14 shows the variation in hole diameter for several h/d ratios as a function of impact velocity. Here the hole diameter predictions are seen to increase to maximum values at impact velocities between 5 and 6 km/s and then begin to slowly decrease. This reversal in hole diameter near impact velocities of 5 to 6 km/s is an inherent characteristic of the model developed herein and is not supported by experimental data. Hence, the model should not be used for impact velocities beyond approximately 6 km/s. It is likely that the reduction in particle velocity according to Eq. (22) is the cause of the reversal in hole diameter. Therefore, future efforts in this area should focus on modifying Eq. (22) so that the reversal in hole diameter is removed.

SUMMARY AND CONCLUSIONS

A one-dimensional formulation has been developed to predict the diameter of the hole created in a thin plate that has been impacted by a spherical projectile. This was accomplished by modeling the creation and attenuation of the Hugoniot impact pressure in a radial direction along the plate surface. The pressure was translated into the thickness of the target by calculating the intersecting position of the advancing shock front and each wave in a centered rarefaction fan. The position where the advancing shock pressure at the center of the target thickness is reduced to a predetermined threshold value is defined to be the hole diameter.

The algorithm was calibrated for aluminum-on-aluminum impacts by determining the threshold or critical pressure from several hundred experimental data points. An analysis of the calibration indicated some inherent short-comings of the basic model and, as a result, two adjustments were added to account for

the effects of very high velocity impacts and very thin target plates. After incorporating these adjustments, a reasonable calibration was obtained for aluminum-on-aluminum impacts on target plates for a variety of relative thicknesses.

The results of this analysis indicate that hole diameters can adequately be predicted using one-dimensional shock physics. The results obtained with the final adjusted model compare favorably against those obtained using a variety of empirical formulations that were previously developed from large sets of experimental data.

ACKNOWLEDGMENTS

The authors are grateful to Mr. Pete Rodriguez and Mr. Scott Hill of the Structural Development Branch (ED52) at the NASA/Marshall Space Flight Center for making the HITS database available for use in this analysis. The authors would like to extend their thanks to Dr. James S. Wilbeck for his guidance, support, and inspiring discussions of shock physics.

REFERENCES

Chou, P. C., "The Strong Plane Shock Produced by Hypervelocity Impact and Late-Stage Equivalence," in W. H. Dittrich, R. J. Eichelberger, and W. W. Atkins, *Proceedings of the Seventh Hypervelocity Impact Symposium*, Vol. II, 1965, Martin Company, Florida, pp. 221–307.

Fowles, G. R., 1960, "Attenuation of the Shock Wave Produced in a Solid by a Flying Plate," *Journal of Applied Physics*, Vol. 31, pp. 655–661.

Gehring, J. W., "Impact on Thin Targets and Shields," in R. Kinslow, *High-Velocity Impact Phenomena*, 1970, Academic Press, New York, pp. 105–156.

Lundeberg, J. F., Stern, P. H., and Bristow, R. J., 1965, "Meteoroid Protection for Spacecraft Structures," NASA Contractor Report 54201.

Madden, R., 1967, "Ballistic Limit of Double-Walled Meteoroid Bumper Systems," NASA Technical Note D-3916.

Maiden, C. J., McMillan, A. R., and Sennett, R. E., 1965, "Thin Sheet Impact," NASA Contractor Report 295.

Nysmith, C. R., 1968, "Penetration Resistance of Double-Sheet Structures at Velocities to 8.8 km/sec," NASA Technical Note D-4568.

Rice, M. H., McQueen, R. G., and Walsh, J. M., "Compression of Solids by Strong Shock Waves," in F. Seitz and D. Turnbull, *Solid State Physics*, Vol. 6, 1958, Academic Press, New York, pp. 1–63.

Schonberg, W. P., Bean, A. J., and Darzi, K., 1991, "Hypervelocity Impact Physics," NASA Contractor Report 4343.

Swale, D. R., 1970, "Hypervelocity Impact on Thin Sheets and Semi-Infinite Targets at 15 km/sec," *AIAA Journal*, Vol. 8, pp. 1240–1244.

Walsh, J. M., Rice, M. H., McQueen, R. G., and Yarger, F. L., 1957, "Shock Wave Compression of Twenty-seven Metals," *Physics Review*, Vol. 108, pp. 196–216.

Walters, W. P., and Scott, R. B., 1985, "The Crater Radial Growth Rate Under Ballistic Impact Conditions," *Computers & Structures,* Vol. 20, pp. 641–648.

Walters, W. P., and Zukas, J. A., 1989, *Fundamentals of Shaped Charges*, John Wiley, New York.

Whipple, F. L., 1947, "Meteorites and Space Travel," *Astronomical Journal*, Vol. 52, p. 137.